Rapid and Parallel Formation of Fe^{3+} Multimers, Including a Trimer, during H-Type Subunit Ferritin Mineralization†

Alice S. Pereira,‡ Pedro Tavares,‡ Steven G. Lloyd,‡ Dana Danger,§ Dale E. Edmondson,*,|| Elizabeth C. Theil,*,§ and Boi Hanh Huynh*,‡

Departments of Physics, Biochemistry, and Chemistry, Rollins Research Building, Emory University, Atlanta, Georgia 30322, and Department of Biochemistry, North Carolina State University, Raleigh, North Carolina 27695

Received February 14, 1997⊗

ABSTRACT: Conversion of Fe ions in solution to the solid phase in ferritin concentrates iron required for cell function. The rate of the Fe phase transition in ferritin is tissue specific and reflects the differential expression of two classes of ferritin subunits (H and L). Early stages of mineralization were probed by rapid freeze-quench Mössbauer, at strong fields (up to 8 T), and EPR spectroscopy in an H-type subunit, recombinant frog ferritin; small numbers of Fe (36 moles/mol of protein) were used to increase Fe^{3+} in mineral precursor forms. At 25 ms, four Fe^{3+}-oxy species (three Fe dimers and one Fe trimer) were identified. These Fe^{3+}−oxy species were found to form at similar rates and decay subsequently to a distinctive superparamagentic species designated the "young core." The rate of oxidation of Fe^{2+} (1026 s^{-1}) corresponded well to the formation constant for the Fe^{3+}− tyrosinate complex (920 s^{-1}) observed previously [Waldo, G. S., & Theil, E. C. (1993) *Biochemistry 32*, 13261] and, coupled with EPR data, indicates that several or possibly all of the Fe^{3+}−oxy species involve tyrosine. The results, combined with previous Mössbauer studies of Y30F human H-type ferritin which showed decreases in several Fe^{3+} intermediates and stabilization of Fe^{2+} [Bauminger, E. R., et al. (1993) *Biochem. J. 296*, 709], emphasize the involvement of tyrosyl residues in the mineralization of H-type ferritins. The subsequent decay of these multiple Fe^{3+}−oxy species to the superparamagnetic mineral suggests that Fe^{3+} species in different environments may be translocated as intact units from the protein shell into the ferritin cavity where the conversion to a solid mineral occurs.

Ferritin is the only protein known to direct a reversible phase transition from a metal ion in solution to a metal ion in a solid matrix (Waldo & Theil, 1996). Bone and tooth formation and resorption processes are formally analogous to the mineralization of ferritin, but a large number of cells and extracellular macromolecules are required for mineralization, in contrast to the case for ferritin. The major role of ferritin in all cells is to concentrate and store iron, since the metal is used in amounts that are effectively $\sim 10^{11}$ times the solubility of the free ion. During oxidative stress or with an iron excess, ferritin appears to protect against radical damage by managing iron−dioxygen interactions (Touati et al., 1995; Balla et al., 1992). The structure of ferritin is common to all known organisms (animals, plants, and microorganisms): a hollow sphere with a diameter of ∼12 nm formed by 24 protein subunits, each of which is a four-helix bundle (Banyard et al., 1978; Harrison & Lilley, 1990; Trihka et al., 1994). The mineral grows and dissolves within the hollow (diameter of ∼8 nm) at the center of the protein (Waldo & Theil, 1996; Harrison & Arosio, 1996).

Rates of ferritin mineralization depend on the ratio of H- and L-type ferritin subunits present in ferritin, which is varied in animals by the differential expression of the two sets of ferritin genes, H and L, in various tissues (Theil, 1987; Harrison & Arosio, 1996; Waldo & Theil, 1996). Studies with recombinant proteins composed of solely H or L subunits have shown that H-type subunits have very fast rates of iron uptake (Fe oxidation and hydrolysis) (Treffry et al., 1993; Waldo et al., 1993) compared to those of L-type subunit proteins; rates differ by more than 100-fold (Waldo & Theil, 1993). Initial rates of mineralization in ferritin from bacteria are also rapid (LeBrun et al., 1993), although slower than the H-subunit ferritin from animals (Waldo & Theil, 1996). The rapid rate of ferritin Fe uptake is accompanied by the transient formation of a Fe^{3+}−tyrosinate complex (Waldo et al., 1993). In general, H-type ferritin subunits predominate in the ferritin of tissues with high oxygen levels (e.g., cardiac and erythroid cells) while L-type ferritin subunits predominate in the ferritin of tissues with slower iron turnover (e.g., liver).

Intermediates in the conversion of hexaquo Fe^{2+} to solid hydrated ferric oxide in ferritin include multimers of Fe^{3+}−oxo complexes bound to the protein, detected by EXAFS and Mössbauer spectroscopy (Yang et al., 1987; Bauminger et al., 1989, 1991, 1993). These earlier studies, however, investigated the properties of Fe^{3+} intermediates at times now known to be long in comparison with the formation time of the initial Fe−protein complex in ferritins composed of H-type subunits. In order to explore the ferritin Fe uptake mechanism and to characterize the type of Fe^{3+} intermediates that form after ferroxidation and during the initial mineral-

† This work was supported in part by National Institutes of Health grants GM 47295 (to B.H.H. and D.E.E.) and DK 20251 (to E.C.T.). S.G.L. is a recipient of a Young Scientist Training Scholarship from the Life and Health Insurance Medical Research Fund. A.S.P. and P.T. are recipients of postdoctoral research fellowships from Programa PRAXIS XXI of Junta Nacional de Investigacao Cientifica e Tecnologica, Portugal.

* Authors to whom correspondence should be addressed.
‡ Department of Physics, Emory University.
§ North Carolina State University.
|| Departments of Biochemistry and Chemistry, Emory University.

⊗ Abstract published in *Advance ACS Abstracts,* June 15, 1997.

S0006-2960(97)00348-6 CCC: $14.00

ization process, recombinant frog H-type subunit ferritin samples were rapidly mixed with oxygenated solutions of Fe^{2+} and quenched by rapid freezing at various times after mixing for Mössbauer spectroscopic investigations. The results show that several multinuclear ($n = 2-3$) $Fe^{3+}-$oxy clusters form in parallel with the rapid oxidation of Fe^{2+}. The rate of the rapid Fe^{2+} oxidation by H-subunit ferritin was determined directly for the first time and was found to be similar to that of the formation of the Fe−tyrosine complex determined earlier using stopped-flow techniques (Waldo & Theil, 1993). These observations demonstrate that multiple processes are involved immediately after the initial oxidation of Fe^{2+} by ferritin and that the purple Fe−tyrosine complex (or complexes) identified previously is an initial product of the oxidation. Further, data of a ferritin sample reacted with Fe^{2+} for 2 days indicate clearly that these initially forming complexes are precursors of the ferritin mineral. Implications of our current findings in relation to ferritin function are discussed.

METHODS

Protein Preparation. H-type subunit frog ferritin was isolated by protein expression using a pET3 vector containing the 5F12 coding sequence (Didsbury et al., 1986) in the *NdeI* site; host *Escherichia coli* BL21-3 cells were grown in medium containing sorbital and betaine (Blackwell & Horgan, 1991). Ferritin synthesis was induced in mid-log cells using IPTG (isothiopropyl thiogalactoside), and the soluble ferritin was isolated, after sonication of the bacterial cells, by FPLC on a Fast Q-Sepharose (Pharmacia) matrix. Protein purified to homogeneity was sterilized by filtration through a 0.45 μm membrane and stored at 4 °C for less than 1 week before mixing with Fe^{2+}.

Preparation of Rapid Freeze-Quenched Samples. Rapid freeze-quenched Mössbauer and EPR samples were obtained using an Update Instruments rapid freeze-quench apparatus following procedures described previously (Ravi et al., 1994). Apoferritin solutions, in 0.2 M MOPS buffer (pH 7) and 0.2 M NaCl, were oxygenated to saturation under 1 atm of O_2 and then rapidly mixed with O_2-saturated $FeSO_4$ solutions, in 0.2 M NaCl, at 23 °C. The protein was allowed to react with the Fe and oxygen for fixed time periods (25 ms to 1 s) before being sprayed into cold isopentane at −140 °C. The frozen samples were packed into either EPR quartz tubes or a Mössbauer delrin cuvette and stored in liquid nitrogen. Mössbauer samples were made with an ^{57}Fe-enriched (≥95% plus enrichment) $FeSO_4$ solution that was prepared from an iron metal foil. The final concentration of Fe was 2 mM for the Mössbauer samples and 2.4 mM for the EPR samples. The Fe/protein molar ratio was kept at 36 in order to maximize the accumulation of the Fe−protein intermediate observed in stopped-flow measurements (Waldo & Theil, 1993). Throughout this paper, the ferritin protein concentrations are expressed as 24-subunit oligomers. Under the reaction conditions of 298 K and 1 atm, O_2 has a solubility of 1.23 mM in water (Dean, 1992). Since the initial concentration of Fe^{2+} after mixing was 2 mM and the Fe/O_2 stoichiometry was determined to be 2.0 for 36 Fe/ferritin (Waldo & Theil, 1993), there is sufficient O_2 to oxidize the iron.

Mössbauer and EPR Spectroscopies. Mössbauer spectra were recorded in either a weak-field spectrometer equipped with a Janis 8DT variable-temperature cryostat or a strong-field spectrometer furnished with a Janis CNDT/SC Super-Varitemp cryostat encasing an 8 T superconducting magnet. Both spectrometers operate in a constant acceleration mode in a transmission geometry. The zero velocity of the spectra refers to the centroid of a room-temperature spectrum of a metallic iron foil. The Mössbauer spectra were analyzed using the WMOSS program (WEB Research Co., Edina, MN) based on a spin Hamiltonian formalism conventionally used for Mössbauer analysis (Huynh, 1994).

EPR data acquisition was performed on a Bruker ER 200D-SRC spectrometer equipped with an Oxford Instrument ESR 910 continuous-flow cryostat. The spectra were recorded at 8 K with a microwave power of 2 mW, a microwave frequency of 9.43 GHz, a modulation frequency of 100 kHz, a modulation amplitude of 1 mT, and a receiver gain of 5×10^4.

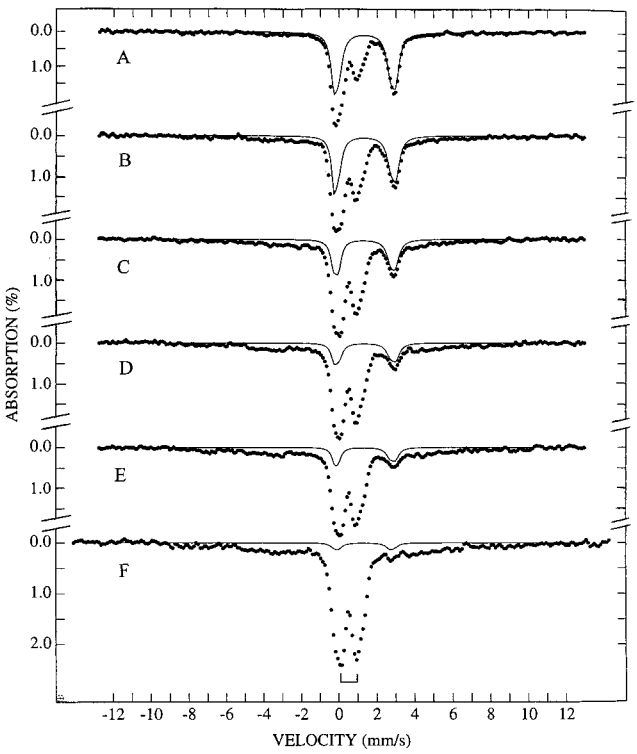

FIGURE 1: Mössbauer spectra of rapid freeze-quenched samples from the reaction of recombinant frog H-type subunit apoferritin with $^{57}Fe^{2+}$ (36 Fe per 24 apoferritin subunits) in the presence of O_2. The data were recorded at 4.2 K with a 50 mT magnetic field applied parallel to the γ-beam. The reaction was quenched at (A) 25 ms, (B) 60 ms, (C) 130 ms, (D) 220 ms, (E) 440 ms, and (F) 1 s. The solid lines are theoretical simulations of the nonreacted Fe^{2+} species (see the text) showing its decay in intensity as a function of reaction time. The bracket indicates the position of the central quadrupole doublet representing the initial forming ferric products of the reaction.

RESULTS

Reaction of Apoferritin with Fe^{2+} and O_2. Figure 1 shows the time-dependent Mössbauer spectra of the reaction of apoferritin (56 μM) with ferrous ions (36 Fe/ferritin molecule) in the presence of O_2. The reaction was freeze-quenched at 0.025, 0.060, 0.13, 0.22, 0.44, or 1 s. The spectra were recorded at 4.2 K with a 50 mT field applied parallel to the γ-beam. The progress of the reaction is clearly visible from these spectra. At the first time point (0.025 s, Figure 1A), the majority of the iron atoms (55%) are in the

unreacted ferrous state, which exhibits a broad quadrupole doublet (solid line in Figure 1A) with parameters (quadrupole splitting $\Delta E_Q = 3.00$ mm/s and isomer shift $\delta = 1.36$ mm/s)[1] typical of high-spin Fe^{2+}. As the reaction time increases, the intensity of this ferrous doublet decreases and, after 1 s of reaction time, is almost unobservable (Figure 1F). Accompanying the decay of the Fe^{2+} species, a broad central doublet (marked by a bracket) increases in intensity. This central doublet is comprised of at least three partially resolved quadrupole doublets with parameters ($\Delta E_Q \approx 0.7-1.7$ mm/s and $\delta \approx 0.5$ mm/s) indicative of high-spin Fe^{3+} (see below). In addition, a broad and undefined spectrum extending from −9 to 9 mm/s is observed to gain intensity with increasing reaction time. These time-dependent spectra therefore demonstrate directly the conversion of Fe^{2+} ions to Fe^{3+} species by ferritin using O_2. In the results which follow, the kinetics of oxidation of Fe^{2+} will be presented first, followed by descriptions of various Fe^{3+} species formed during this process.

Rate of Oxidation of Fe^{2+}. As shown in Figure 1, the high-energy line of the quadrupole doublet arising from the Fe^{2+} species is well resolved from the central doublet, making it possible to accurately estimate the relative absorption intensity of this Fe^{2+} doublet in samples taken at different reaction time points. The oxidation of Fe^{2+} as a function of the reaction time can therefore be followed directly by monitoring the decay of the relative intensity of this doublet, since this intensity depends only upon the Fe^{2+} concentration relative to the total Fe concentration. The results are shown in Figure 2A. The oxidation of the Fe^{2+} ions is found to be biphasic: a fast and a slow phase.

The reaction of apoferritin with Fe^{2+} and O_2 was assumed to have a pseudo-first-order dependence on the Fe^{2+} concentration, and the data were analyzed by using the following equation

$$[Fe^{2+}(t)] = C_1 \exp(-k_1 t) + C_2 \exp(-k_2 t) \qquad (1)$$

(Attempts to fit the data with a second-order equation taking into account the dependence on both Fe^{2+} and oxygen concentrations gave no improvement in the fits.) The solid line plotted in Figure 2A is a least-squares fit to the data using eq 1. The majority of the Fe^{2+} ($C_1 = 72 \pm 3\%$) is oxidized in a fast phase with an apparent pseudo-first-order rate constant k_1 of 28.5 ± 3 s^{-1}, with the remainder ($C_2 = 28 \pm 3\%$) oxidized at a slower pseudo-first-order rate k_2 of 2.3 ± 1 s^{-1}.

Characterization of Fe^{3+} Species Formed during Fe^{2+} Oxidation by Ferritin. To characterize the various Fe^{3+} species formed during the oxidation of Fe^{2+}, it is necessary to deconvolute the Mössbauer spectrum into its spectral components corresponding to the different Fe^{3+} species. This is made difficult by the fact that these components are only partially resolved, and a unique deconvolution cannot be obtained by using a single spectrum alone. Instead, it is necessary to consider, as a whole, the entire set of Mössbauer spectra recorded under wide ranges of temperatures (1.5−100 K) and applied fields (0−8 T) for all the samples

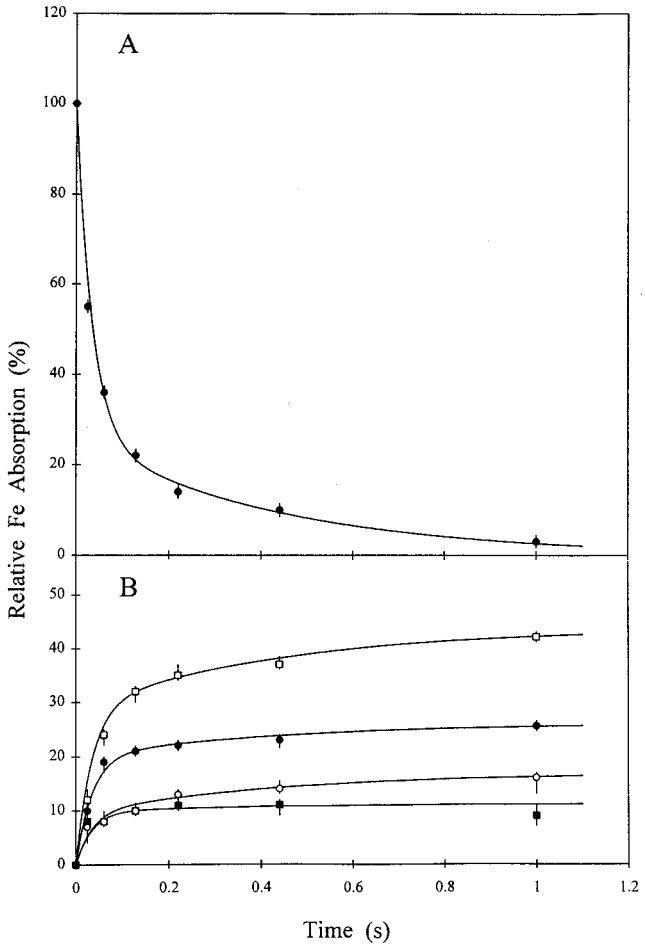

FIGURE 2: Time dependence of all Fe species in the early reaction of H-type subunit apoferritin with Fe^{2+} and O_2, as monitored by Mössbauer spectroscopy. (A) Decay of the Fe^{2+} species and (B) formation of the Fe^{3+} initial products: (●) 0.7 mm/s dimer, (■) 1.2 mm/s dimer, (○) 1.7 mm/s dimer, and (□) trimer. The solid line in panel A is a least-squares fit of eq 1 to the data with a fast rate constant k_1 of 28.5 s^{-1} and a slow rate constant k_2 of 2.3 s^{-1}. The solid lines in panel B are theoretical calculations of eq 2 using the same k_1 and k_2 values (but with varying C_1 and C_2, see the text), indicating the formation of these ferric species parallels that of the decay of the Fe^{2+}.

quenched at different reaction time points. A self-consistent iterative trial and error approach[2] was therefore adopted to obtain a set of spectral components that could satisfactorily explain the entire set of spectra. The results of this analysis are presented below and are represented by the solid lines plotted over the experimental data in Figures 3 and 4 (the contributions from the Fe^{2+} species have been removed from these spectra). The agreement between the experimental spectra and the simulations based on the analysis is excellent.

Due to the complexity of the problem and to avoid confusion, the major findings resulting from the analysis are

[1] At least two quadrupole doublets are required to properly simulate the line shape of the Fe^{2+} doublet. The parameters used in the simulation are as follows: $\Delta E_Q(1) = 3.25$ mm/s, $\delta(1) = 1.36$ mm/s, line width(1) = 0.43 mm/s, $\Delta E_Q(2) = 2.72$ mm/s, $\delta(2) = 1.35$ mm/s, and line width(2) = 0.50 mm/s.

[2] First, the spectra of the 1 s sample, which contains only 3% ferrous species, were analyzed to obtain initial estimates of the characteristic parameters for the various ferric species. These initial estimates were used to simulate spectra of the ferric species, which were then used for removal of the ferric contribution from the spectra of the 25 ms sample (which contains 55% ferrous species) to obtain spectra representing the ferrous species at various experimental conditions. These prepared spectra of the ferrous species were then used for removing the ferrous contributions from spectra of samples of all other time points to obtain the ferric components for a second analysis for refining the parameters. This entire procedure was then repeated until the data and the spectral simulation converged.

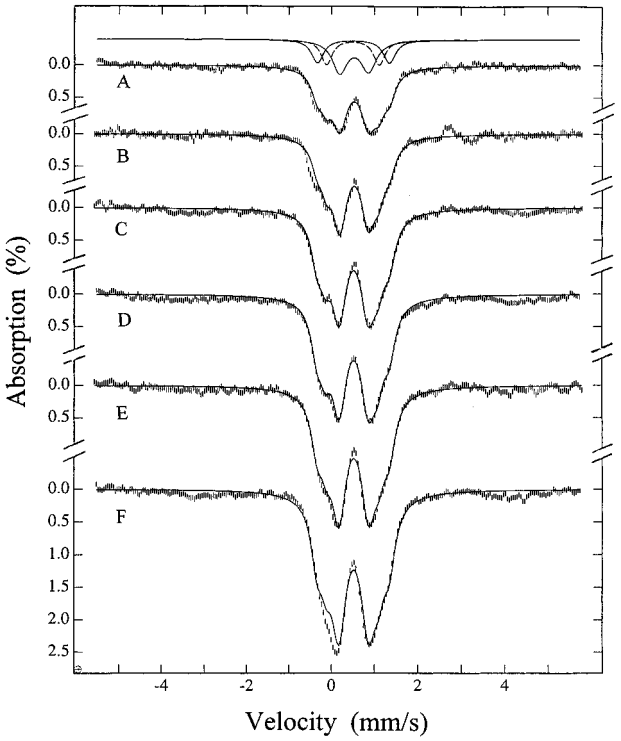

FIGURE 3: Mössbauer spectra at 4.2 K of rapid freeze-quenched samples from the reaction of H-type apoferritin with Fe^{2+} and O_2. These are the same spectra shown in Figure 1 but with the contributions of the Fe^{2+} species (solid lines in Figure 1) removed and with an expanded velocity scale to enhance the resolution at the central region. Outer regions of the spectra are not shown. The two solid lines plotted at the top of the figure represent the 0.7 and 1.7 mm/s quadrupole doublet, and the dashed line is the 1.2 mm/s quadrupole doublets. The solid lines plotted over the data are superpositions of these three quadrupole doublets with varying intensities, indicating that the central region of these spectra can be explained as a composition of these three doublets.

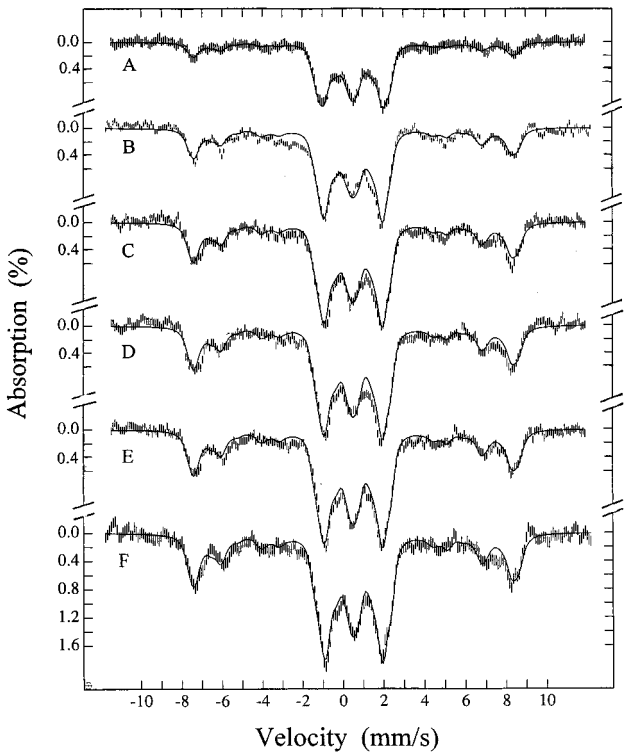

FIGURE 4: Strong-field (8 T) Mössbauer spectra at 4.2 K of rapid freeze-quenched samples from the reaction of H-type recombinant frog apoferritin with Fe^{2+} (36 Fe per 24 apoferritin subunits) and O_2. The field is applied parallel to the γ-beam. The samples are the same as those of Figure 1 which were freeze-quenched at (A) 25 ms, (B) 60 ms, (C) 130 ms, (D) 220 ms, (E) 440 ms, and (F) 1 s after rapid mixing. The contributions of the Fe^{2+} species have been removed from these spectra. The solid lines are superpositions of theoretical simulations of the four initial ferric species using the parameters listed in Table 1 and concentrations listed in Table 2.

summarized here first. Four distinct antiferromagnetically coupled Fe^{3+} species, three dinuclear Fe^{3+} clusters and one trinuclear Fe^{3+} cluster, were identified and represented by four different Mössbauer spectral components. Their characteristic parameters are listed in Table 1. The three dimers can be distinguished by their ΔE_Q values and therefore are labeled accordingly as the 1.7, 1.2, and 0.7 mm/s dimers. The trimer shows a ΔE_Q value similar to that of the 0.7 mm/s dimer. Very little temperature dependence was found for these ΔE_Q values up to 170 K (spectra recorded at a temperature higher than 100 K were collected from a rapidly mixed sample frozen in liquid nitrogen after 2 days of reaction). All four clusters exhibit similar isomer shift value of ~0.5 mm/s indicative of high-spin ferric compounds with oxygen ligands. A more detailed description of the spectroscopic properties of these ferric−oxy species, which explains the above conclusions, is presented below.

To further illustrate the Mössbauer spectral properties of the ferric−oxy species, we show in Figure 3 the same spectra as those shown in Figure 1 but with the contribution from the ferrous species removed and with an expanded scale near the central region, such that it focuses only on this region for improved resolution and the outer parts of the spectra are not shown. At least three quadrupole doublets are observed with similar δ of ≈0.5 mm/s but with varying ΔE_Q values of 0.69, 1.23, and 1.68 mm/s, representing respectively the 0.7, 1.2, and 1.7 mm/s species mentioned above. The 0.7 and 1.7 mm/s doublets are visible as the inner peaks and outer shoulders, respectively (see the solid lines plotted at the top of Figure 3). The 1.2 mm/s doublet is not easy to visualize, but careful spectral decomposition indicates its presence (dashed line plotted at the top of Figure 3). It is clear from the spectra shown in Figure 3 that all three species are present in samples taken at all the reaction time points. While the isomer shifts of these three doublets are indicative of high-spin Fe^{3+} (a Kramers system), the fact that the spectra are quadrupole doublets indicates that all three Fe^{3+}-containing chemical species share a distinctive electronic property. Ferric quadrupole doublets may arise from complexes with an even number of Fe^{3+} ions with strong antiferromagnetic exchange coupling to form a diamagnetic ground state. Alternatively, if the electronic relaxation rate is much faster than the nuclear Lamor precession (~10^{-7} s for an ^{57}Fe nucleus), the magnetic hyperfine interaction will average out, causing Fe^{3+} ions in a Kramers system to exhibit a quadrupole doublet. To distinguish ferric quadrupole doublets arising from exchange-coupled diamagnetic ground state and fast electronic relaxation, the spectra were recorded in the presence of a strong magnetic field. Figure 4 shows the spectra of those same samples shown in Figures 1 and 3 recorded at 4.2 K and in the presence of a parallel field of 8 T. In analogy to the weak-field spectra, the three ferric species also absorb at the central region of the strong-field spectra. The solid lines plotted in Figure 4 are simulations using the parameters (ΔE_Q and δ values) determined from the weak-field spectra and assuming diamagnetism for these three ferric species (i.e., the effective field at the Fe nucleus

Table 1: Mössbauer Parameters for the Initial Ferroxidase Products of H-Type Subunit Ferritin

species	ΔE_Q (mm/s)	δ (mm/s)	η^a	$A/g_n\beta_n{}^b$(T)	line width (mm/s)	spin
0.7 mm/s dimer	$+0.69 \pm 0.04$	0.53 ± 0.02	1.0 ± 0.4	0	0.35	0
1.2 mm/s dimer	-1.23 ± 0.04	0.50 ± 0.02	1.1 ± 0.4	0	0.32	0
1.7 mm/s dimer	-1.68 ± 0.04	0.51 ± 0.02	0.6 ± 0.4	0	0.30	0
trimer,[c] site 1	$+0.7 \pm 0.1$	0.51 ± 0.04	-0.7 ± 0.2	-22.6 ± 0.3	0.5	$^5/_2$
trimer, site 2	-0.7 ± 0.1	0.51 ± 0.04	-1.0 ± 0.2	$+17.4 \pm 0.3$	0.5	$^5/_2$
trimer, site 3	$+0.7 \pm 0.1$	0.51 ± 0.04	-0.2 ± 0.2	-19.1 ± 0.3	0.5	$^5/_2$

[a] $\eta = (V_{xx} - V_{yy})/V_{zz}$ is the asymmetry parameter, where V_{ii} are the principal components of the electric field gradient at the Fe nucleus. [b] A is the magnetic hyperfine coupling constant, and $g_n\beta_n$ is the magnetic moment of the ^{57}Fe nucleus. [c] The trimer is assumed to have a rhombicity parameter E/D of $^1/_3$.

of these species is equal to the applied field). The agreement between experiment and simulations at the central region of the spectra provides definitive evidence for the diamagnetism of these three ferric species. This observed diamagnetism indicates that these ferric species are most probably antiferromagnetically coupled $(Fe^{3+})_2-$oxy clusters. Since a dinuclear Fe^{3+} cluster may contain iron sites with different ligand environments, it is possible for a single dinuclear cluster to exhibit two quadrupole doublets as observed in the R2 subunit of the *E. coli* ribonucleotide reductase (Lynch et al., 1989). A comment is therefore in order here to address the question of whether these doublets observed in ferritin may represent different iron sites of a single dinuclear cluster. A necessary criterion for assigning two quadrupole doublets to two iron sites of a dinuclear iron center is that the two doublets must have the same intensity, which is the case for ribonucleotide reductase. Since the three doublets observed in ferritin have different intensities, they cannot represent signals arising from different iron sites of a single dinuclear center. Furthermore, this difference in intensity also cannot be explained as being due to different occupations of the iron sites when coupled with the observed diamagnetism of the doublets, because only a fully occupied diiron center would exhibit diamagnetism. A monomeric Fe^{3+} (a diiron center lacking one iron), on the other hand, is paramagnetic. Consequently, the only possible assignment for the three quadrupole doublets observed in ferritin is that they represent three distinct $(Fe^{3+})_2-$oxy clusters.

The Mössbauer spectral properties of the Fe^{3+} trimer are more complex. Its electronic relaxation is neither very fast nor slow on the time scale of the nuclear Larmor precession frequency, resulting in the broad and ill-defined magnetic spectral component observed in the 4.2 K weak-field spectra (Figure 1). This makes spectral analysis difficult. The problem can be overcome by collecting the spectra under strong applied fields for at fields of sufficient strength (i.e., strong enough so that the magnetically purturbed electronic ground state becomes stabilized by an energy of $>kT$ relative to the excited states) the spectra of a slow-relaxing species and a fast-relaxing species converge to the same spectral profile. We have therefore collected spectra with varying applied fields. With increasing field strengths, the broad and unresolved magnetic features sharpen into recognizable lines as seen in the outer region of the spectra shown in Figure 4. Figure 5 shows the magnetic spectral component corresponding to the Fe^{3+} trimer recorded at 4, 6, and 8 T applied fields. These spectra were prepared from those of the 1 s sample by removing the contributions from the ferrous species and the three Fe^{3+} dimers. The 1 s sample was used primarily because it contains the least amount of ferrous species, of which the spectral properties as a function of applied fields

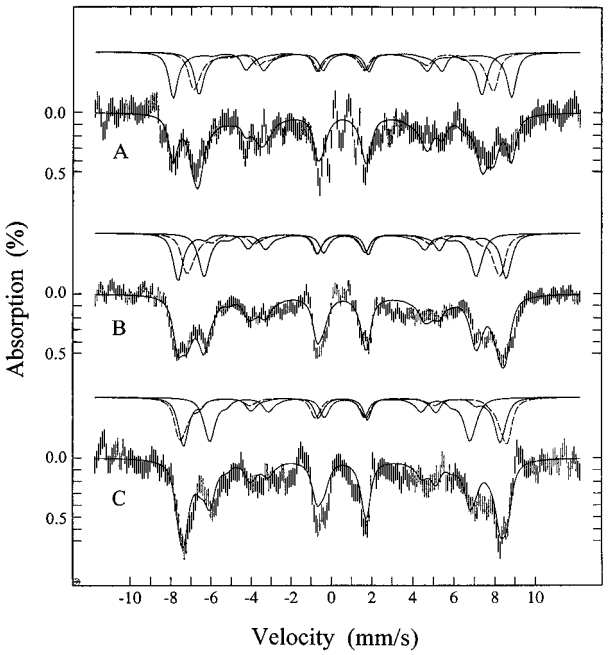

FIGURE 5: Field-dependent Mössbauer spectra of the trimer recorded at 4.2 K. The experimental spectra are prepared from spectra of the 1 s sample recorded with a magnetic field of (A) 4 T, (B) 6 T, or (C) 8 T applied parallel to the γ-beam. The solid lines plotted over the experimental spectra are superpositions of theoretical spectra of the three Fe sites of the trimer simulated with the parameters listed in Table 1. Simulations for the individual Fe sites are also plotted above each corresponding experimental spectrum: sites 1 and 3, solid lines; and site 2, dashed line.

are least understood. Consequently, any "possible" distortion of the prepared magnetic spectrum caused by "improper" removal of the ferrous contribution is minimized by the use of the 1 s sample. The spectral behavior of the three Fe^{3+} dimers as a function of the applied field can be accurately simulated because they are diamagnetic and because their ΔE_Q and δ values have been determined from the weak-field spectra. The spectra shown in Figure 5 can be explained as superpositions of three magnetic spectral components of equal intensity corresponding to three Fe^{3+} sites of an exchange-coupled cluster (i.e., a trinuclear Fe cluster). The cluster spin is assumed to be $^5/_2$ as supported by the $g = 4.3$ resonance in the EPR spectrum discussed below. The antiferromagnetically coupled nature of the cluster is indicated unambiguously by the variation of the total magnetic splittings of the component spectra with applied field strength. The total splittings for two of the three components (solid lines plotted above the spectra in Figure 5) decrease with increasing applied field strengths. This behavior is generally expected for an ^{57}Fe nucleus, since the magnetic hyperfine constant A for Fe ions is negative,

i.e., the strong internal hyperfine field opposes the weaker applied field, resulting in the decrease of the effective field at the Fe nucleus with increasing applied field strengths. However, the splitting of the third component (dashed lines plotted above the spectra of Figure 5) increases with increasing applied field strengths. This could happen only if the corresponding Fe atom is antiferromagnetically coupled to other Fe atoms such that its intrinsic spin is antiparallel to the system spin, resulting in an apparent positive magnetic hyperfine *A* value (Huynh et al., 1980; Kent et al., 1980). Since the field-dependent behavior of one of the magnetic components indicates the presence of antiferromagnetic coupling and since coupling of two ferric ions would not yield a half-integer spin system, all three iron sites corresponding to the three magnetic components must be involved in the exchange coupling. In other words, the three magnetic spectral components must represent three iron sites of an exchange-coupled cluster, i.e., a trinuclear Fe^{3+}cluster. Inspection of the outer regions of the spectra shown in Figure 4 indicates clearly that this trimer is present in all the samples quenched at different reaction times.

Rates of Formation of the Fe^{3+} Species Resulting from Fe^{2+} Oxidation by Ferritin. The analysis described above provides an accurate estimate of the relative absorption intensity of each of the four ferric species in the samples in addition to yielding information concerning the nuclearity and electronic properties of the ferric clusters. The formation of these Fe^{3+} species as a function of the reaction time can therefore be obtained with the results shown in Figure 2B. Similar to the oxidation of the Fe^{2+} species, the formation of these four Fe^{3+} clusters is also biphasic. The data suggest that all four species are formed simultaneously, instead of sequentially, with rates similar to those of the decay of the Fe^{2+} species. To illustrate this point, formation curves (solid lines) for the four species are plotted in Figure 2B using eq 2 and rate constants (k_1 = 28.5 s^{-1} and k_2 = 2.3 s^{-1}) determined for the decay of the Fe^{2+} species.

$$C(t) = C_1[1 - \exp(-k_1 t)] + C_2[1 - \exp(-k_2 t)] \quad (2)$$

Parameter C_1 and C_2 used in the calculations for the 1.7 mm/s dimer, 1.2 mm/s dimer, 0.7 mm/s dimer, and trimer are, respectively, 9.6 and 7.3%, 10 and 1.2%, 20 and 6%, and 28.8 and 14.8%. The agreement between the calculations and the experimental data demonstrates that within experimental uncertainties the four Fe^{3+} clusters form in parallel with the decay of the Fe^{2+} species. In other words, multiple processes are involved immediately following the oxidation of ferrous ions by ferritin. Multiple Fe^{3+} species, similar to those reported here (see Discussion), have previously been observed 0.5, 10, or 20 min after mixing Fe^{2+} with human recombinant H-type subunit ferritin in the presence of O_2 (Bauminger et al., 1989, 1991, 1993). The ferric species identified in the studies of recombinant human ferritin have been interpreted to show a precursor/product relationship (Bauminger et al., 1993). The field-dependent Mössbauer data on rapid freeze-quench samples presented here, however, show clearly that these ferric species form simultaneously, at least in frog H-type subunit ferritin, and that the multiple oxidation products occur as early as 25 ms after mixing Fe^{2+} and protein.

EPR spectroscopy of Rapidly Forming Species in H-Subunit-Type Ferritins. The rapid freeze-quench method was used to prepare samples for EPR investigations in parallel with the samples for Mössbauer measurements in order to explore more completely the properties of the paramagnetic species observed in the Mössbauer measurements. Samples were made with 2.4 mM Fe and the same 36/1 Fe/ferritin ratio. The samples were quenched at reaction times of 0.025, 0.045, 0.10, 0.25, 0.44, and 1 s. Two EPR signals were detected at low temperature (8 K), one at $g = 4.3$ and one at $g = 2.0$ (data not shown). The shape of the EPR signal at the $g = 2.0$ region suggests a protein-based radical. A similar signal has been observed in human recombinant H-type subunit ferritin and has been reported previously (Yu et al., 1995). The $g = 4.3$ signal is typical of mononuclear Fe^{3+} in a low-symmetry environment with an *E/D* of $^1/_3$ and an *S* of $^5/_2$. However, an exchange-coupled system with an odd number of Fe^{3+} ions could also form a ground state with an *S* of $^5/_2$. Since the Mössbauer data presented above show only one paramagnetic species, namely, the trimer, there is no other alternative but to assign the $g = 4.3$ signal to the trimer. Absolute quantification of the $g = 4.3$ signal was not attempted since the signal arises from an excited state of the $S = {}^5/_2$ multiplet, making its quantitation difficult without *a priori* knowledge of the multiplet fine structure splittings. Nevertheless, the relative intensity of the $g = 4.3$ EPR signal as a function of reaction time can be compared with the time dependence of the trimer formation obtained from the Mössbauer measurements (Figure 6). Although the EPR data show a large scattering (probably due to variation in the sample density), the comparison of EPR and Mössbauer data suggests that the time course of the $g = 4.3$ EPR signal intensity conforms with the formation of the trimer.[3]

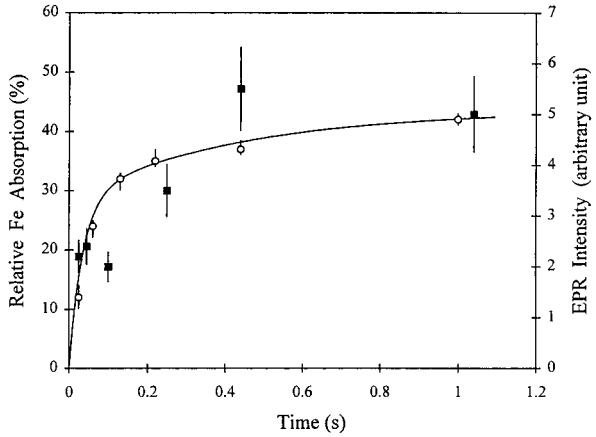

FIGURE 6: Comparison of the time course of the EPR $g = 4.3$ signal intensity (filled squares) with the formation of the trimer (empty circles) observed by Mössbauer spectroscopy. The EPR data were recorded at 8 K with a microwave power of 2 mW (see Methods for other experimental conditions). The Mössbauer data and the solid curve are the same of those presented in Figure 2.

Formation of the Polynuclear Fe^{3+} Cluster by H-Type Subunit Ferritin at 36 Fe/Protein. To investigate whether H-type subunit ferritin is capable of forming a large polynuclear ferrihydrite mineral core at small Fe loading and to examine whether the above-mentioned small ferric species are transient during ferritin mineralization, apoferritin was

[3] An EPR sample was prepared with apoferritin rapidly mixed with Fe^{2+} and O_2 and allowed to react aerobically for 2 days. The sample exhibits the same EPR signal at $g = 4.3$ with a reduction in intensity consistent with the decrease of the amount of the trimer determined from Mössbauer measurements of the Mössbauer 2-day-old sample.

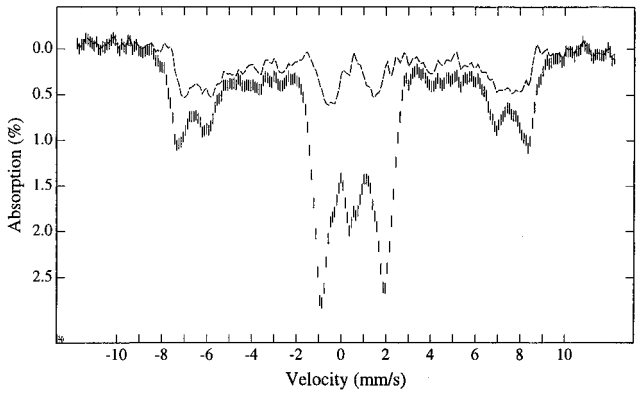

FIGURE 7: Mössbauer spectrum of a sample of H-type frog apoferritin rapidly mixed with 36 equiv of Fe^{2+} in the presence of O_2 and frozen 2 days after mixing. The spectrum (vertical bars) was recorded at 4.2 K with an 8 T magnetic field applied parallel to the γ-beam. The dashed line shows the spectrum of the young mineral at 8 T (see the text for the preparation of this spectrum).

rapidly mixed with Fe^{2+} (36 Fe/protein) in the presence of O_2 and allowed to react aerobically for 2 days at 4 °C before freezing at 77 K for Mössbauer measurements. Figure 7 shows a Mössbauer spectrum of the 2-day-old sample recorded at 4.2 K with a parallel applied field of 8 T. Spectral components associated with the above-mentioned Fe^{3+} dimers and trimer are clearly observable. However, their relative absorption intensities are reduced in comparison with those of the 1 s sample (see Table 2). Except for the 0.7 mm/s dimer, the reduced levels of the other species are outside of the experimental errors. Removal of the contributions of these small ferric clusters reveals a complex magnetic spectrum (dashed line in Figure 7, representing ≈32% of the total Fe absorption or approximately 12 Fe/ferritin on average) that can be attributed to larger ($n > 3$) polynuclear ferric clusters.

A typical ferritin mineral would have detectable superparamagnetism (St. Pierre et al., 1986). Even as few as 10 Fe/ferritin formed a readily detectable superparamagnetic ferric species in an L-subunit-type ferritin (Yang et al., 1987). In order to demonstrate that superparamagnetic species are indeed present in the 2-day-old H-subunit ferritin sample, spectra were recorded at various temperatures with a weak or in the absence of an applied field. The 40 and 4.2 K spectra of the 2-day-old sample are shown in Figure 8 (spectra A and B, respectively). In addition to the spectral components of the four small clusters (the 0.7, 1.2-, and 1.7 mm/s dimers and the trimer) seen at shorter reaction times, a broad magnetic sextet spectral component is visible in the 4.2 K spectrum (Figure 8B), suggesting the presence of larger clusters. Since the relative concentrations of the small initial forming clusters in the 2-day-old sample can be determined from the 8 T spectrum (Figure 7), and since the spectral properties of these small clusters can be obtained from the spectra of the 1 s sample recorded under the same experimental conditions, their contributions can be removed from the 4.2 K spectrum of the 2-day-old sample to reveal the spectral component corresponding to the larger clusters. Figure 8C shows such a prepared spectrum with a broad sextet magnetic pattern displaying a distribution of internal magnetic field of 45−46 T. At 40 K, however, this sextet spectrum is not visible and has collapsed into a quadrupole doublet that is unresolved from the other quadrupole doublets (Figure 8A). Such a temperature dependence is typical for superparamagnetic systems. Due to the presence of multiple species in the 2-day-old sample and the relatively small contribution of the superparamagnetic species, the blocking temperature[4] of the superparamagnetic species could not be determined. However, the fact that the spectrum collapses at 40 K indicates that these superparamagnetic clusters have a blocking temperature much lower than that of a mature ferritin mineral core; the blocking temperature of mature horse spleen ferritin reconstituted with 480 Fe/protein had been determined to be 38 K (Yang et al., 1987). Since the blocking temperature is proportional to the average size of the superparamagnetic particles, the observed lower blocking temperature suggests that these superparamagnetic clusters in the 2-day-old sample are much smaller than the mature ferritin core, and may represent polynuclear ferric clusters formed in the early stage of ferritin mineralization. Thus, these clusters are designated the *young ferritin core* and are characterized by a blocking temperature of below 40 K and a distribution of internal fields at 45−46 T.

DISCUSSION

The first step in the formation of the iron mineral in ferritin is oxidation of Fe^{2+} to Fe^{3+}. Mainly indirect methods have been used until recently to analyze rates of ferroxidation by ferritin, especially for fast (H-subunit-type) ferritin. Such methods have included measurement of the decrease in the formation of the ferrous 1,10-phenanthroline complex (Macara & Harrison, 1973), appearence of polynuclear ferric−oxo species (absorbance in the 330−420 nm range) [e.g., Bryce and Crichton (1973), Macara et al. (1973), and Mertz and Theil (1983)], acceleration of formation of ferric−transferrin in acetate buffer (Baker & Boyer, 1986), formation of purple ferric−tyrosine (Waldo et al., 1993), and generation of EPR active ferric complexes (Hanna et al., 1991; Sun & Chasteen, 1994). Besides being indirect, additional limitations exist for these methods. In the case of using the chelator 1,10-phenanthroline, the method does not always distinguish the oxidation of Fe^{2+} from the inaccessible Fe^{2+} [e.g., Rohrer et al. (1989)]. EPR spectroscopy is limited by the inability to detect all the ferric species present such as the diamagnetic Fe^{3+} dimers observed in this work. In general, methods depending on the appearance of Fe^{3+} in a particular environment are limited by the necessary assumption that the species measured is the initial oxidation product, which is not necessarily the case. Thus, while the ferric−tyrosine forms rapidly (Waldo & Theil, 1993), for example, it could be a product of an even faster forming colorless ferric species that is the initial ferroxidation product.

Here, we adopted an approach that combined the rapid freeze-quench method and Mössbauer spectroscopy to investigate in detail the oxidation of Fe^{2+} ions by H-type subunit ferritin. Application of the rapid freeze-quench method allowed us to quench the ferroxidation reaction at various time points along the reaction pathway for spectroscopic investigations. The time resolution of the rapid freeze-quench method is in the millisecond range, much shorter than what was possible in previous Mössbauer measurements (Yang et al., 1987; Bauminger et al., 1989, 1991, 1993). A major advantage of using Mössbauer

[4] The blocking temperature is defined as the temperature where half of the iron absorption is in a magnetic sextet and half is in a quadrupole doublet.

Table 2: Percentage of the Total Fe Absorption of the Ferric Species Formed at Various Reaction Times, t_R, during Mineralization of H-Type Subunit Ferritin[a]

t_R	0.7 mm/s dimer	1.2 mm/s dimer	1.7 mm/s dimer	trimer	young mineral
25 ms	10 (8−11)	8 (7−10)	7 (4−9)	12 (10−14)	0
60 ms	19 (17−20)	8 (7−10)	8 (7−10)	24 (22−25)	0
130 ms	21 (20−22)	10 (9−12)	10 (9−11)	32 (30−33)	0
220 ms	22 (21−23)	11 (10−12)	13 (12−14)	35 (34−37)	0
440 ms	23 (21−24)	11 (9−12)	14 (13−16)	37 (36−39)	0
1 s	26 (25−27)	9 (7−11)	16 (13−17)	42 (41−43)	<5
48 h	24 (23−28)	6 (3−7)	9 (8−10)	29 (22−30)	32 (29−35)

[a] The values in the parentheses represent the estimated range of possible percent values for each species at t_R.

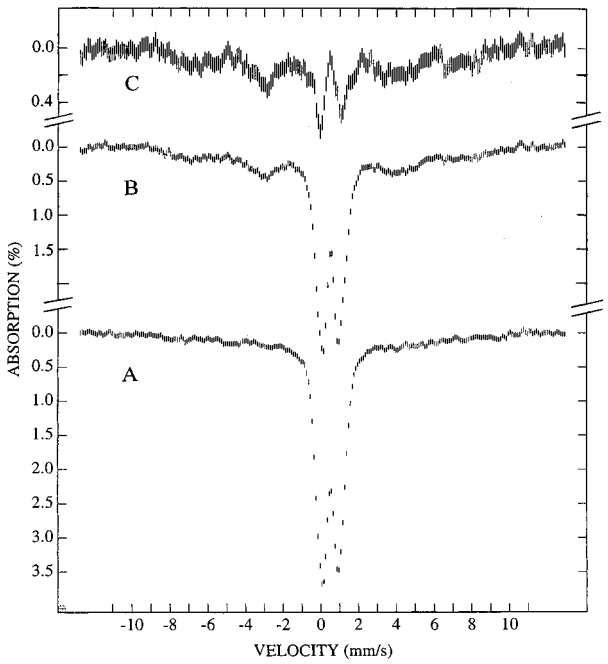

FIGURE 8: Temperature dependence of the Mössbauer spectrum of the 2-day-old sample of Figure 7. The spectra were recorded at (A) 40 K with zero field and (B) 4.2 K with a 50 mT parallel field. The sextet magnetic spectrum shown in part C is prepared from the 4.2 K spectrum of part B by removing the contributions of the trimer and dimers, the percent absorptions of which are determined from the 8 T spectrum (see the text).

spectroscopy for this study is that it can detect and characterize all the Fe species present in the sample. Consequently, a combined approach can measure directly the time course of the fast oxidation of the Fe^{2+} ions, as well as the formation of all the initial and subsequent oxidation products. Furthermore, these products can be characterized spectroscopically. The pseudo-first-order rate constant k_1 for the oxidation of Fe^{2+} by the H-type subunit ferritin with 36 Fe/protein loading was determined directly, for the first time, to be 28.5 s^{-1}. Although the function of ferritin in oxidizing Fe^{2+} ions in solution and in storing the oxidized products inside the hollow protein shell has been known for decades, evidence for direct involvement of specific amino acid side chains in the ferroxidation process has only recently been obtained when Waldo and Theil (1993) observed a fast-forming purple ferric−tyrosinate species using stopped-flow UV−vis spectroscopy. Converting the apparent ferrous oxidation rate (28.5 s^{-1}) determined in this work to the rate of oxidation ($k_{ox} = k_1$[Fe]/[ferritin]) as defined by Waldo and Theil (1993) yields an oxidation rate of 1026 s^{-1}, which compares very well with the rate constant of 920 s^{-1} determined for the formation of the ferric−tyrosinate complex measured at 550 nm (Waldo & Theil, 1993). This observation demonstrates unambiguously that the ferric−tyrosinate complex formed is the initial product (or among the initial products) of Fe^{2+} oxidation in this fast ferritin ferroxidation and therefore establishes that tyrosine residues are involved in H-type subunit ferritin function.

In a weak applied field, the initial ferric products of ferroxidation by recombinant frog H-type subunit ferritin exhibit three different-intensity quadrupole doublets with a similar isomer shift of 0.5 mm/s but different quadrupole splittings of 0.7, 1.2, and 1.7 mm/s. Similar quadrupole doublets have also been found previously for the ferroxidation products of the human H-type subunit ferritin (Bauminger et al., 1989, 1991, 1993). On the basis of the similarity with the Mössbauer spectra of known μ-oxo dinuclear Fe^{3+} clusters in several proteins (Lynch et al., 1989; DeWitt et al., 1991; Fox et al., 1993), the Fe^{3+} species with ΔE_Q values of 1.2 and 1.7 mm/s were assigned to represent two oxo-bridged $(Fe^{3+})_2$ clusters (Bauminger et al., 1989, 1991). The assignment was suggested to be supported by X-ray crystallographic structures of mammalian H-subunit-type ferritin (Lawson et al., 1991) and bacterial ferritin (Hempstead et al., 1994), which show a possible metal binding site similar to those found in μ-oxo diiron cluster-containing proteins, such as ribonucleotide reductase (Nordlund et al., 1990) and soluble methane monooxygenase (Rosenweig et al., 1993). Such dinuclear ferric systems are antiferromagnetically coupled and invariably have a diamagnetic ground state. Observation of quadrupole doublets is consistent with the Fe^{3+} ions being in a diamagnetic environment since no internal field is expected for diamagnetic systems. However, in the presence of a weak applied field or in the absence of a magnetic field, quadrupole doublets can also be observed for Fe atoms in a paramagnetic system if the relaxation between thermally accessible electronic states is fast in comparison with the nuclear precession time, which would average out the internal field. In other words, Mössbauer spectra measured under the weak-field conditions used previously would not be able to distinguish these two very different electronic properties. Application of a strong applied field at low temperature would resolve these two situations. For a paramagnetic system, the ground electronic multiplet would be split by the presence of the strong applied field, and at low temperature, only the lowest ground state within the multiplet will be appreciably populated, resulting in a non-zero internal field, which is therefore distinguishable from a diamagnetic system. Furthermore, application of strong magnetic fields would reveal the nuclearity and spin coupling nature of a paramagnetic Fe cluster (Huynh et al., 1980). A major factor that distinguishes the current investigation from previous Mössbauer studies is that strong magnetic fields (up to 8 T) are applied for the measurements.

The ferric species with ΔE_Q values of 1.2 and 1.7 mm/s were found to be indeed diamagnetic, providing direct evidence that they are antiferromagnetically coupled dinuclear Fe^{3+} clusters. The nature of the quadrupole doublet with a ΔE_Q of 0.7 mm/s, previously assigned to represent larger "clusters" of Fe ($n > 3$), is more complicated.

Examination of the species with a ΔE_Q of 0.7 mm/s at strong magnetic fields (4−8 T) reveals the presence of two species, one diamagnetic and one paramagnetic, an unexpected finding according to conclusions made previously on the basis of data obtained at weak fields (Bauminger et al., 1989, 1991, 1993). The diamagnetism of one of these species strongly suggests that this species is yet another antiferromagnetically coupled dinuclear Fe^{3+} cluster. Strong-field Mössbauer spectra further reveal that the paramagnetic species is composed of three antiferromagnetically coupled Fe^{3+} ions. Correlating the Mössbauer results with EPR measurements on samples prepared under similar conditions suggests that the Fe^{3+} trimer has a system spin of $^5/_2$ and exhibits EPR signals indistinguishable from that of a monomeric Fe^{3+} species. In fact, such an EPR signal with a formation rate very similar to that of the trimer has been reported during the reconstitution of recombinant human H-type subunit ferritin and was attributed to monomeric ferric species (Sun & Chasteen, 1994). However, on the basis of our current findings, it is very likely that the EPR signal detected in the human H-type subunit ferritin during the early stage of ferroxidation reaction may also represent a Fe^{3+} trimer similar to that observed in frog ferritin. A trimeric Fe^{3+}−oxy model complex exhibiting a typical $S = {}^5/_2$, $g =$ 4.3 EPR signal and magnetic hyperfine coupling constants similar to those of the trimer reported here has been reported recently (Bill et al., 1997).

The ΔE_Q values of μ-oxo diferric clusters are typically large, within the range of 1.4−2.4 mm/s (Kurtz, 1990; Que & True, 1990). The small ΔE_Q of 0.7 mm/s found for the diamagnetic dinuclear Fe^{3+} species formed in ferritin may indicate a μ-hydroxo cluster (Kurtz, 1990) or represent a local Fe environment resembling that in the ferritin mineral core which exhibits a similar ΔE_Q value (St. Pierre et al., 1986; Yang et al., 1987). A similar quadrupole doublet has been observed previously in horse spleen ferritin and recombinant human H-type mutants and was assigned as small superparamagnetic ferric clusters (Bauminger et al., 1991, 1993). Since the samples examined in these studies were not prepared with rapid mixing−rapid quench techniques and were frozen at reaction times (minutes to hours) much longer than those of the current study (except for the 2-day-old sample), it is possible that small superparamagnetic ferric clusters have been formed. However, in view of our current finding that various Fe^{3+} species in ferritin (the 0.7 mm/s dimer, trimer, and mineral core) exhibit a similar 0.7 mm/s quadrupole doublet, it is very likely that the doublet observed in these previous studies could represent a mixture of species, particularly in samples taken at the early reaction time points.

The parallel formation of all four ferric oxy clusters coincident with the oxidation of the Fe^{2+} ions is a unique observation of the current study. Their formations are all biphasic with a fast and a slow rate similar to that of the decay of the Fe^{2+} ions. This observation strongly suggests that multiple processes are involved following the oxidation of ferrous ions by H-type subunit ferritin and that all four ferric species are initial oxidation products. At first glance, this observation of multiple ferric species appears to be at odds with the studies of X-ray crystallography (Lawson et al., 1991; Hempstead et al., 1994) and of site-directed mutants of H-subunit-type ferritin (Sun et al., 1993; Yu et al., 1995; Harrison & Arosio, 1996), which suggest that fast Fe^{2+} oxidation occurs at a single proposed diiron binding site. However, it is important to point out that ferritin, as the only protein which directs the conversion of ferrous ions in solution into forming the solid iron mineral core in the ferritin cavity, has unique functional features. Our results indicate that immediately following the ferrous oxidation several types of multimeric ferric species form exceedingly fast and at the same rates. The results neither support nor refute the presence of a single ferroxidation site. It is not yet clear which sites are the sites for the multiple initial oxidation products. However, it is interesting to note that mutation of Y30[5] eliminates several of these Fe^{3+}−oxy species (Bauminger et al., 1993; also, see below) and that Y30 is a conserved residue near the proposed dinuclear ferroxidation center. If there were indeed a single ferroxidation site in each H-type ferritin subunit, as suggested by the work of X-ray crystallography (Lawson et al., 1991; Hempstead et al., 1994) and of site-directed mutants (Sun et al., 1993; Yu et al., 1995; Harrison & Arosio, 1996), our results may reflect the flexibility of the site since it is able to accommodate various initial oxidation products. Considering the ferritin function, this flexibility is not surprising and may be important since these initial oxidation products would have to be eventually translocated into the protein cavity. The plasticity of ferritin has been noted in a previous protein crystallography study (Trikha et al., 1995).

There are several possible explanations for why the oxidation is observed to be biphasic. One explanation would be that there are two subtypes of ferritin in our samples such that one reacts faster and the other slower. In order for this hypothesis to explain the observed biphasic curve in these samples, however, the Fe^{2+} must bind tightly to the "slow" ferritin, for otherwise the "fast" ferritin would oxidize essentially all the Fe^{2+} ions within ≈0.2 s. Also, in order to explain the parallel formation of the four oxidation products, both the fast and slow ferritin molecules would have to catalyze the oxidation reaction with the same four parallel processes. This appears to be rather unlikely. A more plausible explanation based on ferritin function is a classical burst reaction (Bender et al., 1966) which assumes a fast initial step followed by a much slower rate-limiting conversion of the initial product into the final product. In the case of ferritin, the slow step could be the conversion of these initially forming small ferric clusters into a solid phase mineral core, which involves transporting and recombining these clusters into larger polynuclear clusters. Such an explanation is supported by the measurements on the 2-day-old samples which indicate that larger polynuclear clusters have been formed at the expense of the smaller initially forming clusters (Table 2).

The similarity of the rate of formation of ferric−tyrosinate species (920 s^{-1}) detected by optical spectroscopy (Waldo & Theil, 1993) with the rate of oxidation of the Fe^{2+} (1026

[5] Two numbering systems have been used for ferritin sequences. In the numbering system introduced by Lawson et al. (1991), 4 is added to the original sequence assignement. Thus, Y30F is equal to Y34F in Bauminger et al. (1993).

s^{-1}) determined here indicates that the ferric−tyrosinate species is an initial oxidation product. The current Mössbauer measurements indicate that there are four initial oxidation products in the form of small ferric clusters. Taken together, these observations suggest that there is a high probability that more than one, if not all, of the small ferric−oxy clusters are coordinated to protein tyrosine residues. This assignment of the small Fe^{3+}−oxy species to the ferric−tyrosine species, which show an absorption maximum at 550 nm, is consistent with that observed for purple acid phosphatases which exhibit an absorption maximum between 550 and 570 nm (Doi et al., 1988). Spectroscopic investigations of rapid freeze-quenched samples of site specific mutants of conserved tyrosine residues should help to elucidate the location of the sites of these initial Fe^{3+}−oxy−tyrosinate clusters. Earlier Mössbauer studies on recombinant human H-type subunit ferritin (Bauminger et al., 1993) showed that substitution of tyrosine 30 for phenylalanine (Y30F) eliminated the 0.7 and 1.62 mm/s (corresponding to the 1.7 mm/s doublet in frog ferritin) doublets in samples prepared 0.5 and 30 min after mixing of Fe^{2+} with protein. Note that the 0.7 mm/s doublet was assigned to larger ($n > 3$) ferric clusters. But, since strong-field measurements needed to fully characterize the Fe^{3+} species were not performed, it is probable that a mixture of ferroxidase products (i.e., the 0.7 mm/s dimer, the trimer, and the young ferritin core) may be contributing to the 0.7 mm/s doublet. Thus, assuming that the 0.7 mm/s dimer and the trimer are also part of the initial ferroxidase products in the human H-subunit ferritin, the reported Mössbauer data on the Y30F mutant, which show an absence of the 1.62 and 0.7 mm/s doublets at 1 min of reaction time (Bauminger et al., 1993), suggested that Y30 is involved in the formation of the trimer, the 0.7 mm/s dimer, and the 1.7 mm/s dimer. Stopped-flow UV−vis studies showed that Y30F substitution slows the rates of mineralization in human H-subunit ferritin (Treffrey et al., 1995) and of ferric−tyrosine formation in frog H-subunit ferritin (Fetter, Cohen, Sander-Loehr, and Theil, to be published). These observations can be explained by our finding that multiple processes are taking place following ferritin ferroxidation and by the suggestion that residue Y30 is involved in most but not all the processes. Multiple postferroxidation processes occurring at different protein sites (or a flexible site) also explain previous results of site-directed mutagensis of human H-subunit ferritin which altered the rate of ferroxidation but did not inhibit ferritin function completely (Sun et al., 1993; Bauminger et al., 1993; Treffry et al., 1995).

Multiple parallel oxidation pathways in H-subunit ferritin provide an alternate model in contrast to that previously proposed (Bauminger et al., 1989, 1991, 1993). The earlier model, based on Mössbauer data collected at limited and longer time points (basically 0.5 and 30 min; Bauminger et al., 1993) and on site-directed mutations at the 3-fold channel (Treffry et al., 1993), suggested that ferrous ions are to be oxidized at a single ferroxidase site in the interior of the four-helix bundle to form dinuclear Fe^{3+}−oxo clusters (i.e., the 1.2 and 1.7 mm/s dimers). The Fe^{3+}−oxo dimers are split into monomers, which are then transported from the ferroxidation site to the 3-fold channels and then to the cavity in the center of the protein to form the solid ferritin mineral core. The proposed initial formation of the Fe^{3+}−oxo dimers is supported by our rapid freeze-quench Mössbauer data, but the proposed subsequent event of spliting the dimers into monomers appears to be energetically unfavorable since dinuclear Fe^{3+}−oxo clusters are stable compounds and the proposal is inconsistent with our data which show an absence of monomeric Fe^{3+} species. Our data suggest that the initial postoxidation of Fe^{2+} by H-ferritin involves multiple processes and that the final formation of the ferritin mineral requires transporting, followed by combining the initially formed Fe^{3+}−oxy clusters, because (1) the formation of the trimer and various Fe^{3+} dimers occurs in parallel with the oxidation of Fe^{2+} ions, (2) no monomeric ferric species were observed in our rapid freeze-quench samples and the 2-day-old sample, (3) the observed biphasic behavior of the ferrous oxidation and initial cluster formation is consistent with fast formation of initial products at one or more protein sites followed by a slow process of transporting the initial products to the nucleation site(s), (4) fast ferroxidase activity is restored very slowly after the addition of the initial group of Fe^{2+} ions (Waldo & Theil, 1993; Treffry et al., 1995), which reflects the slow process of vacating the ferroxidase and/or the postoxidation sites, and (5) the young ferritin mineral core is formed at the expense of the initially forming Fe^{3+}−oxy clusters. Finally, using small ferric−oxy clusters as building blocks to form larger clusters is energetically possible and has been observed in model compound studies (Gorun & Lippard, 1986; Nair & Hagen, 1992; Taft et al., 1993; Caneschi et al., 1995).

The multiplicity of ferric clusters which form in the initial stages of mineralization, as observed by rapid freeze-quench Mössbauer spectroscopy, emphasizes the relatively unspecific Fe−protein interactions in ferritin compared to proteins in which the metal is part of a catalytic center required for function. In ferritin, the metal is a substrate for oxidation and transport. Whether each of the 24 subunits in ferritin has "active sites" for binding, oxidizing, and/or transporting Fe ions across the protein to and from the cavity, or the sites are formed in regions between neighboring subunits, or a single subunit may have multiple types of metal binding sites cannot be determined at the current level of knowledge; on the basis of the kinetic Mössbauer data presented here for the multiple ferric species observed with 36 Fe added per protein, there are an average of 10−12 sites per ferritin molecule (24 subunits). There appears to be no strong evolutionary pressure on ferritin for a single process for Fe oxidation and transfer across the protein. Rather, the main requirement for ferritin mineralization may be protein folding and packing which produce an accessible interior hollow in which formation of a solid phase mineral core can occur. Illustrations of "minimalist" ferritin structures include (1) a quadruple Glu/Ala-mutated L-subunit ferritin which folds and assembles correctly (Trihka et al., 1994, 1995) but lacks protein-based ferroxidase or nucleation sites (Wade et al., 1991; Trihka et al., 1995; Waldo & Theil, 1996) and (2) a form of concanavalin A which assembles with an interior hollow in the protein (Yariv et al., 1988). Both proteins form a polynuclear ferric−oxo species *in vitro*. Evolutionary nuances, crucial to biology, that are indicated by the specificity of genetic control of expression of H and L subunits apparently include the acquisition of Fe transport paths in ferritin with increasing speed, but the protein assembly to form a commodious interior space, common to both H- and L-subunit ferritin, clearly dominates.

ACKNOWLEDGMENT

The authors are grateful to Dr. Geoffrey S. Waldo for his contributions to the initial experiments of this work and to Mr. Joel C. Verbist for his assistance in collecting some of the strong-field Mössbauer spectra.

REFERENCES

Baker, G. R., & Boyer, R. F. (1986) *J. Biol. Chem. 261*, 13182−13185.
Balla, G., Jacob, H. S., Balla, J., Rosenberg, M., Nath, K., Apple, F., Eaton, J. W., & Vercellotti, G. M. (1992) *J. Biol. Chem. 267*, 18148−18153.
Banyard, S. H., Stammers, D. K., & Harrison, P. M. (1978) *Nature 271*, 282−284.
Bauminger, E. R., Harrison, P. M., Nowik, I., & Treffry, A. (1989) *Biochemistry 28*, 5486−5493.
Bauminger, E. R., Harrison, P. M., Hechel, D., Nowik, I., & Treffry, A. (1991) *Proc. R. Soc. London, Ser. B 244*, 211−217.
Bauminger, E. R., Harrison, P. M., Hechel, P. M., Hodgson, N. W., Nowik, I., Treffry, A., & Yewdall, S. (1993) *Biochem. J. 296*, 709−719.
Bender, M. L., Begué-Cantón, M. L., Blakeley, R. L., Brubacher, L. J., Feder, J., Gunter, C. R., Kézdy, F. J., Killheffer, J. V., Jr., Marshall, T. H., Miller, C. G., Roeske, R. W., & Stoops, J. K. (1966) *J. Am. Chem. Soc. 88*, 5890−5913.
Bill, E., Krebs, C., Winter, M., Gerdan, M., Trautwein, A. X., Flörke, U., Haupt, H.-J., & Chaudhuri, P. (1997) *Chem. Eur. J. 3*, 193−201.
Blackwell, J. R., & Horgan, R. A. (1991) *FEBS Lett. 295*, 10−12.
Bryce, C. F. A., & Crichton, R. R. (1973) *Biochem. J. 133*, 301−309.
Caneschi, A., Cornia, A., Fabretti, A. C., & Gatteschi, D. (1995) *Angew. Chem., Int. Ed. Engl. 34*, 2716−2718.
Dean, J. A. (1992) *Lang's Handbook of Chemistry*, p 57, McGraw-Hill, New York.
DeWitt, J. G., Bentsen, J. G., Rosenzweig, A. C., Hedman, B., Green, J., Pilkington, S., Papaefthymiou, G. C., Dalton, H., Hodgson, K. O., & Lippard, S. J. (1991) *J. Am. Chem. Soc. 113*, 9219−9235.
Didsbury, J. R., Theil, E. C., Kaufman, R. E., & Dickey, L. F. (1986) *J. Biol. Chem. 261*, 949−955.
Doi, K., Antanaitis, B. C., & Aisen, P. (1988) *Struct. Bonding (Berlin) 70*, 3−26.
Fox, B. G., Hendrich, M. P., Surerus, K. K., Andersson, K. K., Froland, W. A., Lipscomb, J. D., & Münck, E. (1993) *J. Am. Chem. Soc. 115*, 3688−3701.
Gorun, S. M., & Lippard, S. J. (1986) *Nature 319*, 666−668.
Hanna, P. M., Chen, Y., & Chasteen, N. D. (1991) *J. Biol. Chem. 266*, 886−893.
Harrison, P. M., & Lilley, T. H. (1990) in *Iron Carriers and Iron Proteins* (Loehr, T. M., Ed.) pp 353−452, VCH, New York.
Harrison, P. M., & Arosio, P. (1996) *Biochim. Biophys. Acta 1275*, 161−203.
Hempstead, P. D., Hudson, A. J., Artymiuk, P. J., Andrews, S. C., Banfield, M. J., Guest, J. R., & Harrison, P. M. (1994) *FEBS Lett. 350*, 258−262.
Huynh, B. H. (1994) *Methods Enzymol. 243*, 523−543.
Huynh, B. H., Moura, J. J. G., Moura, I., Kent, T. A., LeGall, J., Xavier, A. V., & Münck, E. (1980) *J. Biol. Chem. 255*, 3242−3244.
Kent, T. A., Huynh, B. H., & Münck, E. (1980) *Proc. Natl. Acad. Sci. U.S.A. 77*, 6574−6576.
Kurtz, D. M., Jr. (1990) *Chem. Rev. 90*, 585−606.
Lawson, D. M., Artymiuk, P. J., Yewdall, S. J., Smith, J. M. A., Livingstone, J. C., Treffry, A., Luzzago, A., Levi, S., Arosio, P., Cesareni, G., Thomas, C. D., Shaw, W. V., & Harrison, P. M. (1991) *Nature 349*, 541−544.
LeBrun, N. E. L., Cheesman, M. R., Thomson, A. J., Moore, G. R., Andrews, S. C., Guest, J. R., & Harrison, P. M. (1993) *FEBS Lett. 323*, 261−266.
Lynch, J. B., Juarez-Garcia, C., Münck, E., & Que, L., Jr. (1989) *J. Biol. Chem. 264*, 8091−8096.
Macara, I. G., Hoy, T. G., & Harrison, P. M. (1973) *Biochem. J. 135*, 343−348.
Mertz, J. R., & Theil, E. C. (1983) *J. Biol. Chem. 258*, 11719−11726.
Nair, V. S., & Hagen, K. S. (1992) *Inorg. Chem. 31*, 4048−4050.
Nordlund, P., Sjöberg, B. M., & Eklund, H. (1990) *Nature 345*, 593−598.
Que, L., Jr., & True, A. E. (1990) in *Progess in Inorganic Chemistry: Bioinorganic Chemistry* (Lippard, S. J., Ed.) Vol. 38, pp 97−200, John Wiley & Soms, Inc., New York.
Ravi, N., Bollinger, J. M., Jr., Huynh, B. H., Edmondson, D. E., & Stubbe, J. (1994) *J. Am. Chem. Soc. 116*, 8007−8014.
Rohrer, J. S., Frankel, R. B., Papaefthymiou, G. C., & Theil, E. C. (1989) *Inorg. Chem. 28*, 3393−3395.
Rosenweig, A. C., Frederick, C. A., Lippard, S. J., & Nordlund, P. (1993) *Nature 366*, 537−543.
St. Pierre, T. G., Bell, S. H., Dickson, D. P. E., Mann, S., Webb, J., Moore, G. R., & Williams, R. J. P. (1986) *Biochim. Biophys. Acta 870*, 127−134.
Sun, S., & Chasteen, N. D. (1994) *Biochemistry 33*, 15095−15102.
Sun, S., Arosio, P., Levi, S., & Chasteen, N. D. (1993) *Biochemistry 32*, 9362−9369.
Taft, K. L., Papaefthymiou, G. C., & Lippard, S. J. (1993) *Science 259*, 1302−1305.
Theil, E. C. (1987) *Annu. Rev. Biochem. 56*, 289−315.
Touati, D., Jacques, M., Tardat, B., Bouchard, L., & Despied, S. (1995) *J. Bacteriol. 177*, 2305−2314.
Treffry, A., Bauminger, E. R., Hechel, D., Hodson, N. W., Nowik, I., Yewdall, S. J., & Harrison, P. M. (1993) *Biochem. J. 296*, 721−728.
Treffry, A., Zhao, Z., Quail, M. A., Guest, J. R., & Harrison. P. M. (1995) *J. Biochemistry 34*, 15204−15213.
Trihka, J., Waldo, G. S., Lewandowski, F. A., Theil, E. C., Weber, P. C., & Allewell, N. M. (1994) *Proteins 18*, 107−118.
Trihka, J., Theil, E. C., & Allewell, N. M. (1995) *J. Mol. Biol. 248*, 949−967.
Wade, V. J., Levi, S., Arosio, P., Treffry, A., Harrison, P. M., & Mann, S. (1991) *J. Mol. Biol. 221*, 1443−1452.
Waldo, G. S., & Theil, E. C. (1993) *Biochemistry 32*, 13261−13269.
Waldo, G. S., & Theil, E. C. (1996) in *Comprehensive Supramolecular Chemistry* (Suslick, K. S., Ed.) Vol. 5, pp 65−89, Pergamon Press, Oxford, UK.
Waldo, G. S., Ling, J., Sanders-Loehr, J., & Theil, E. C. (1993) *Science 259*, 796−798.
Yang, C.-Y., Meagher, A., Huynh, B. H., Sayers, D. E., & Theil, E. C. (1987) *Biochemistry 26*, 497−503.
Yariv, J., Kalb, A. J., Helliweg, J. R., Papiz, M. Z., Bauminger, E. R., & Norwik, I. (1988) *J. Biol. Chem. 263*, 13508−13510.
Yu, C.-B., Harrison, P. M., Treffry, A., Quail, M. A., Arosio, P., Santambrogio, P., & Chasteen, N. D. (1995) *Biochemistry 34*, 7847−7853.

BI970348F